Ab initio study of the ideal shear strength and elastic deformation behaviors of B2 FeAl and NiAl

Tianshu Li, J. W. Morris, Jr., and D. C. Chrzan
Department of Materials Science and Engineering, University of California, Berkeley, California 94720, USA
and Materials Science Division, Lawrence Berkeley National Laboratory, Berkeley, California 94720, USA
(Received 27 June 2005; revised manuscript received 10 October 2005; published 13 January 2006)

The elastic deformation behaviors of perfect NiAl and FeAl are investigated using an *ab initio* electronic structure total energy method. The calculated ideal shear strengths for the $\{112\}\langle 111\rangle$ and $\{110\}\langle 111\rangle$ slip show qualitatively different features between the two intermetallics. In NiAl, the shear deformation can be understood by exploring the transition among different stress-free structures on the strain paths, while in FeAl the instabilities under shear are found to be dictated by filling of the unstable anti-bonding *d* states. The failure modes under uniaxial $\langle 100\rangle$ tension are also explored for NiAl and FeAl using two methods, a straightforward comparison of the resolved shear stress with the ideal shear strength and a detailed examination of the internal stability condition. Both methods yield the same conclusion: FeAl fails by tension while NiAl fails by shear. These predictions are consistent with the experimentally observed cleavage behaviors.

DOI: 10.1103/PhysRevB.73.024105 PACS number(s): 61.50.Lt, 62.20.Dc, 71.20.Lp

I. INTRODUCTION

The B2 transition-metal aluminides TM-Al (TM=Fe, Co, Ni) are of considerable technological interest for high temperature structural applications and have attracted much attention, both in experiment and theory. On one hand, the similarities in both the crystal structures and the electronic structures lead to some common properties such as high strength, relatively low density, and high melting point, etc. On the other hand, these intermetallics manifest significant differences in their cleavage behaviors.[1–3] These alloys thus compose a fascinating system that allows testing of various hypotheses regarding the origins of the divergence in macroscopic properties.

Although many theoretical efforts have been devoted to this topic, some uncertainties still remain. Physical quantities such as charge density, ionicity, and directional bonding were found to be correlated loosely with the observed behaviors,[4] while differences in their ground-state electronic structures seemed to be inconsequential as far as cleavage behavior was concerned.[5] Interestingly, examining these properties for a strained state might provide useful information that cannot be resolved when only the ground state is considered.[6] Toward this end, study of the ideal strength might shed some light on this topic. Ideal strength calculations offer insight into the connection between the variation of the intrinsic properties such as chemical bonding and symmetry, and the macroscopic mechanical properties of the material.[7]

Prior study of the ideal tensile strength revealed the inherent weakness of B2 FeAl when pulled along $\langle 100\rangle$ direction as compared with CoAl and NiAl.[6] The unique weakness of FeAl in this specific direction has been explained by moving and filling of the anti-bonding $dd\sigma$ orbitals based on a rigid band model. The calculated ideal strengths correlate well with the experimentally observed cleavage behaviors in FeAl and NiAl. This is not surprising in the sense that the cleavage involves breaking atomic bonds and the local stress must be sufficient to overcome the cohesive strength of material, hence a particularly low strength in one specific direction may result in the cleavage anisotropy.

In this work, calculations of the theoretical shear strengths of FeAl and NiAl as well as the examination of the internal stability conditions under the uniaxial $\langle 100\rangle$ tension are conducted in order to understand systematically the ideal deformation behavior of these compounds. It is demonstrated that ideal strength calculations for these intermetallic compounds provide direct insight into their cleavage tendencies.

II. METHOD OF CALCULATION

The calculations are carried out using density functional theory within the local density approximation and using Vanderbilt ultra-soft pseudopotentials[8] as embodied in the Vienna *Ab initio* Simulation Package (VASP).[9] A cut-off energy of 30 Ry and $14\times14\times14$ *k*-points generated by Monkhorst-Pack scheme[10] are chosen to ensure that the calculated total energy converges to within 1 mRy per atom.

The uniaxial ideal stress-strain relation is computed through the following procedure:[11] A fully relaxed unit cell with three orthogonal lattice vectors a_i^0 $(i=1,2,3)$ is uniformly distorted in such a manner that the deformation along direction j on plane i is fixed to a given engineering strain ε_{ij}. There is more than one definition of the finite shear strain; we choose it to be the symmetric part of the deformation tensor

$$\varepsilon_{ij} = \tfrac{1}{2}[D_{ij} + D_{ji}],$$

where the deformation tensor D_{ij} relates the distorted lattice vector a_i' to the undistorted lattice vector a_j^0 by

$$a_i' = a_i^0 + D_{ij}a_j^0.$$

Then the other five strain components are adjusted until their conjugated stress components are relaxed (<0.05 GPa). The only nonzero component σ_{ij} gives the quasi-static stress associated with the engineering strain ε_{ij}.

 ©2006 The American Physical Society

In analogy to studies of body centered cubic (BCC) materials, two shear deformation paths are examined in this calculation: $\{112\}\langle 111\rangle$ and $\{110\}\langle 111\rangle$. $\{112\}\langle 111\rangle$ shear preserves the monoclinic structure but the deformation is asymmetric with respect to the shear direction, i.e., $(\bar{1}\bar{1}2)[111]$ produces a different stress-strain relationship from the opposite direction $(\bar{1}\bar{1}2)[\bar{1}\bar{1}\bar{1}]$. In BCC crystals, the two directions are distinguished by "easy" and "hard" as it takes smaller strain to approach an energy saddle point structure body-centered tetragonal in the easy direction than a based-centered orthorhombic in the hard.[12,13] Consequently a shear in the easy $\{112\}\langle 111\rangle$ gives rise to a lower ideal strength. It should be noted that the conventions used here are irrelevant to the "soft" and hard single crystals defined based on the flow stress in the literature.[14] These classifications are adopted in the current B2 system despite the different crystal structure. In contrast, slip on $\{110\}\langle 111\rangle$ follows a triclinic path, but the two shear directions are symmetric.

The detailed study of the elastic stability of the $\langle 100\rangle$ uniaxial tension path is examined following the internal stability condition derived by Morris *et al.*[15] The symmetrized Wallace tensor $[\lambda_{ij}]$ is required to be positive definite for a crystal to maintain its stability. In other words, the minimum eigenvalue of the symmetric Wallace tensor has to be positive. Since the eigenvector associated with the first vanished eigenvalue indicates the direction of failure, one can fully solve the elastic instability along any deformation path by monitoring the variations of six eigenvalues. However, it should be noted that the statement above is only a necessary condition of stability and material may fail due to other types of instabilities, e.g., a phonon instability,[16] that could be broken prior to the internal instability. These instabilities are not discussed in present work.

A tetragonal uniaxial stretch of a cube along $\langle 100\rangle$ can be described by six independent components λ_{ij} (Ref. 15)

$$\lambda_{11} = C11 + \sigma, \quad \lambda_{12} = C12 - \frac{\sigma}{2}, \quad \lambda_{55} = C55 + \frac{\sigma}{2},$$

$$\lambda_{ij} = Cij \quad (ij = 22,23,44),$$

where C is the elastic constant and σ is the applied uniaxial tensile stress. By computing the elastic constants for different tensile strains, it is straightforward to solve for the eigenvalues of the Wallace tensor.

III. RESULTS AND DISCUSSIONS

A. Ideal strength

The calculated stress and energy increase are plotted as functions of the engineering shear strain for NiAl in Fig. 1. The negative shear strain corresponds to the hard direction (left branch of the curve) in $\{112\}\langle 111\rangle$ shear. In spite of the different paths in shear, the stress-strain curves coincide at the initial loading stage due to the fact that any uniaxial shear in a $\langle 111\rangle$ direction share the same relaxed modulus in the cubic crystal. In the easy direction (right branch of the curve), the two paths diverge as the shear strain increases but

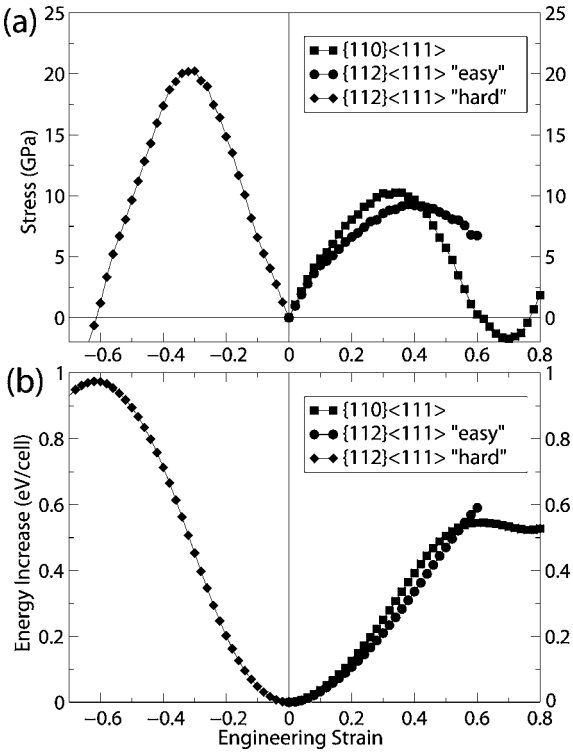

FIG. 1. (a) Stress and (b) energy increase per unit cell vs engineering shear strain for $\{112\}\langle 111\rangle$ and $\{110\}\langle 111\rangle$ shear in NiAl.

at the critical shear strain (0.36–0.38), both curves reach their maximum (~10 GPa), roughly one-half of the ideal shear strength in the $\{112\}\langle 111\rangle$ hard direction.

It is noted that although the B2 structure bears some resemblance to BCC crystal, significant differences in the symmetry constraints that govern the shear instability play a key role in differentiating its ideal deformation behavior. In BCC metals, a stress-free body-centered tetragonal (BCT) saddle point structure is encountered when the crystal is uniaxially sheared around 33% in $\{112\}\langle 111\rangle$ easy direction thus the ideal shear strength emerges at about half way around, i.e., ~16%. The ideal strength in the hard direction is dictated by another stress-free face-centered orthorhombic (FCO) structure. Even though these saddle point structures are not reachable in either the real or ideal world, they act as attractors on the energy surface and they affect the shape of the curve as well as the maximum.

While the B2 crystal behaves in a similar manner as BCC in the $\{112\}\langle 111\rangle$ hard direction in which a body-centered orthorhombic saddle point structure (strain=62%) governs the ideal strength, a closer examination on the crystal structures reveals a different evolution path in the easy direction. With a different type of atom sitting on the body center, the B2 crystal does not have the BCT saddle point structure that dominates three different uniaxial strain paths in BCC, i.e., $\{112\}\langle 111\rangle$ shear on the easy direction, $\{110\}\langle 111\rangle$ shear, and the $\langle 001\rangle$ tension following an orthorhombic path.[13] If the B2 crystal had exactly followed the shear path in BCC on the $\{112\}\langle 111\rangle$ easy slip, a base-centered orthorhombic (BCO) structure would be encountered eventually at a shear strain around 29%. However, calculation shows a nonzero stress

TABLE I. Details in the crystal structures of NiAl at the stress-free states in {110}⟨111⟩ shear.

	Structure	First nearest neighbor		2nd nearest neighbor		Third nearest neighbor	
		Type/#	Distance (Å)	Type/#	Distance (Å)	Type/#	Distance (Å)
Ground state	SC/B2	D[a]/8	2.45	S[b]/6	2.84		
Meta-stable	Mono.	D/6	2.45	S/6	2.68		
Saddle point	Mono.	D/4	2.42	D/2	2.53	S/2	2.62

[a]D stands for the different type.
[b]S stands for the same type.

tensor if this BCO is extracted, hence it is not a saddle point structure on the energy surface. In fact, the crystal evolves along a different path wherein the BCO structure does not even appear, and the shear stress keeps increasing until 38% engineering strain where a maximum strength of 9.3 GPa is reached.

Owing to the same reason, shear in {110}⟨111⟩ also manifests differences from BCC structures. Two stress-free structures appearing on the strain path at the engineering strain 62% and 77% correspond to a saddle point and a local minimum on the energy surface, respectively. The cubic symmetry is reduced to triclinic as the shear strain is applied, but the two extrema are found to be associated with local configurations of relatively high symmetry, i.e., monoclinic. Calculations show that the two monoclinic structures not only differ by their shapes, but essentially, by their numbers of the nearest neighbors (see Table I). At ground state, i.e., B2, each atom has eight first nearest neighbors (FNN) of the different type and six second nearest neighbors (SNN) of the same type which are only 14% more distant than FNNs. At the metastable state, the number of FNNs is reduced to six but all have the same interatomic distance as in the ground state. The number of SNNs is fixed but the interatomic distance is decreased to 2.68 Å. On average, the crystal structure is more dense. The saddle point structure, on the other hand, has a moderately compact structure with both fewer FNNs and SNNs and it is not stable. It then follows the stability of the stress-free structures increases with the coordination number thus NiAl prefers a "sharing" metallic structure.

Figure 2 illustrates the stress-strain and energy-strain relationship for FeAl in shear. A comparison between FeAl and NiAl shows the resemblance in their shear behaviors along {112}⟨111⟩ hard direction (left branch) but a dramatic difference along the easy direction (right branch)-not only the critical strains in FeAl on both paths differ from those in NiAl, but the shapes of the stress-strain curves for two materials are also very dissimilar. On both shear paths in FeAl, the stresses approach their maximum values at the same engineering strain around 0.2 and then drop sharply afterwards. Examination in the geometry evolution demonstrates that the deformations in [111] shear include substantial elongation along the z (or [001]) direction, along which about 14% tensile strains are achieved on both paths when stresses reach their maximum values. Interestingly, such amount of elongation along ⟨100⟩ coincides with the critical tensile strain in uniaxial ⟨100⟩ tension of FeAl.[6] This fact, along with the unusual shape of the stress-strain curves near the maximum region, raises the conjecture that the shear instability along the ⟨111⟩ direction should be attributed to the same mechanism governing the ⟨100⟩ tension.

A comparison in the electronic structures for the two different deformation paths confirms this suspicion. Although degeneracy varies due to different symmetries, two band structures [Figs. 3(a) and 3(b)] share the common feature that the seventh energy band, that is mainly constructed from the anti-bonding $dd\sigma$ along X-M, falls to the Fermi level at the critical strain. This feature can also be seen in the projected density of states (PDOS) for the $d_{3z^2-r^2}$ orbitals which form the $dd\sigma$ bonds between transition metal atoms along z direction. In both ⟨111⟩ shear and ⟨100⟩ tension, the PDOS peak (1.5 eV above the Fermi level) that corresponds to the anti-bonding $dd\sigma$ at the ground state [Fig. 4(a)], moves down to the Fermi level at the critical strains [Figs. 4(b) and 4(c)]. Filling of the anti-bonding d states would destabilize the crystal thus causing weakness, as suggested in the study of the ⟨100⟩ uniaxial tension in FeAl.[6] As a comparison, the

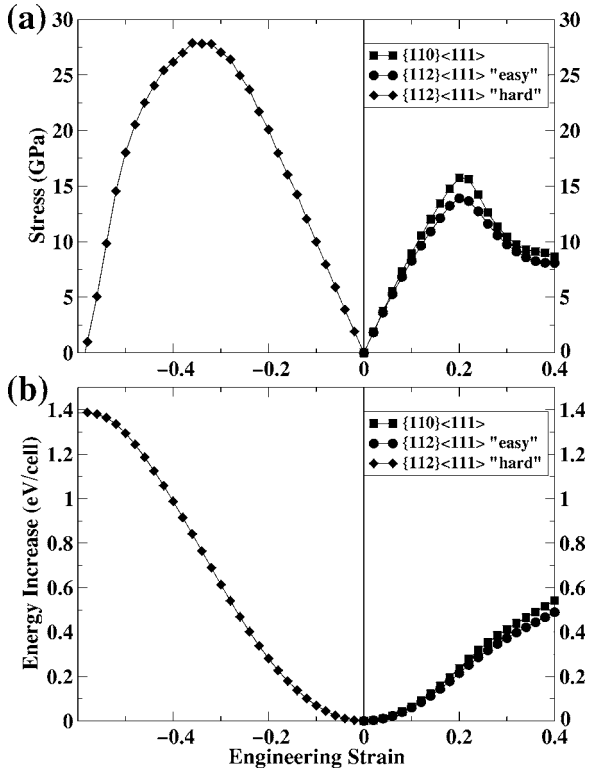

FIG. 2. (a) Stress and (b) energy increase per unit cell versus engineering shear strain for {112}⟨111⟩ and {110}⟨111⟩ shear in FeAl.

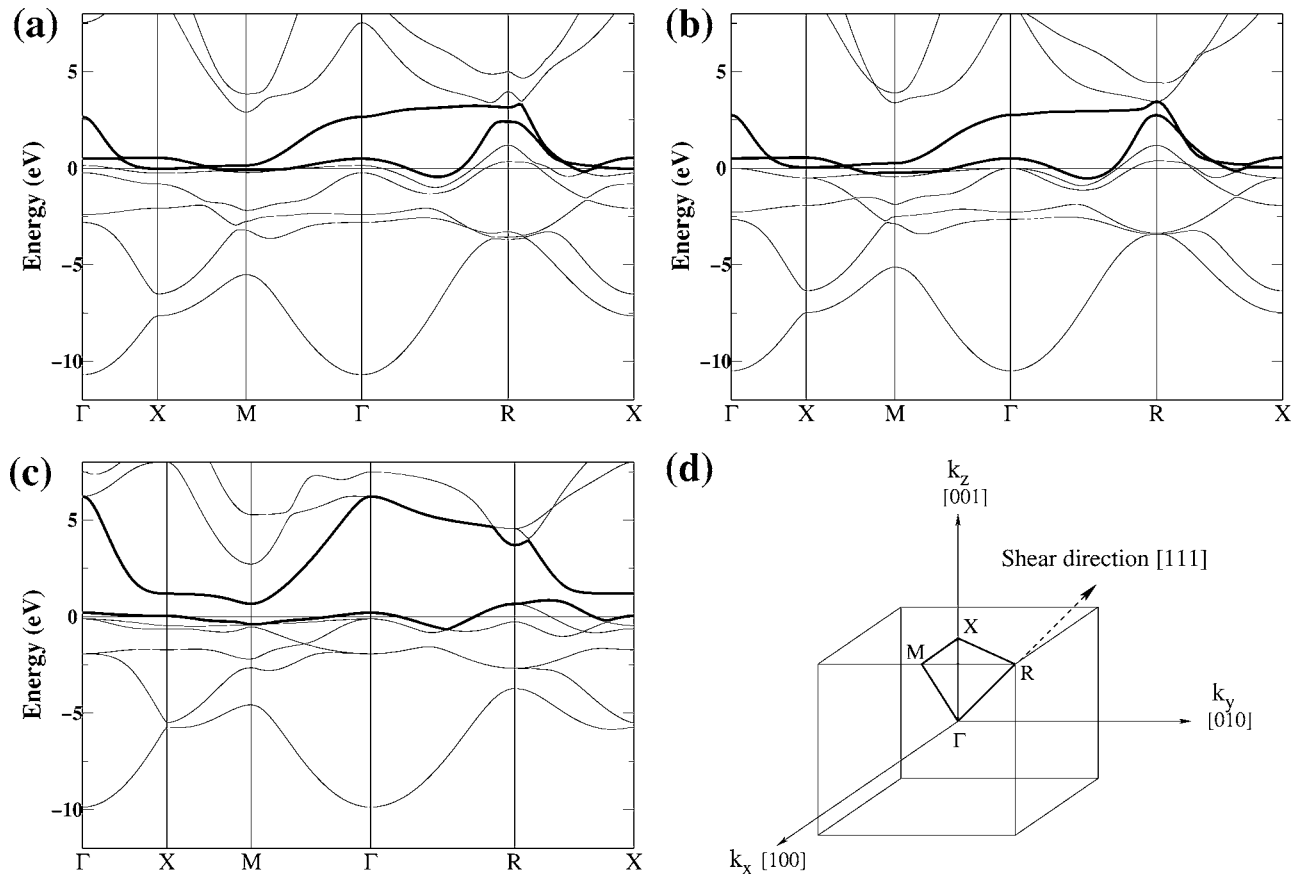

FIG. 3. Calculated band structures of FeAl at instabilities show similarity in (a) $(1\bar{1}0)[111]$ shear and (b) [001] tension. In both cases the elongations of the unit cell along z direction approach 14%. In contrast, the main distortion in (c) [111] tension takes place along the body diagonal ([111]) so that the elongation in z direction is far less obvious. For convenience, the k-points are all labeled using the Brillouin zone of the simple cubic (d).

band structure and PDOS for a uniaxial tension in ⟨111⟩ direction are also given [Figs. 3(c) and 4(d)] and do not show such feature. This is due to the fact that the bond length associated with the $dd\sigma$ states in ⟨111⟩ tension deviated to a degree far less than those in ⟨100⟩ tension or ⟨111⟩ shear. In fact the instability in this direction is dictated by symmetry. The calculation hence suggests an entirely different type of the instability of FeAl as compared to NiAl when uniaxially sheared in ⟨111⟩ direction.

To our knowledge, no prior uniaxial ideal shear strength calculation was attempted in FeAl and NiAl. However, an estimate of the shear strength based on the generalized stacking fault (GSF) model[17] were made by Medvedeva *et al.*[18] in the same system. The critical shear strengths were reported to be 13.3 and 18.1 GPa for {110}⟨111⟩ slip in NiAl and FeAl, respectively, which are higher than 10.3 and 15.7 GPa in our calculations. The discrepancy is attributed to the different loading conditions applied on the materials. In GSF model, a rigid shift of one-half the crystal relative to the other by vector $\vec{u}$ is assumed thus no relaxation is allowed in the calculation, whereas in uniaxial shear the relaxations on orthogonal directions are fundamental to the magnitude of the strength. While we have not explored the influence from the triaxial stress in transition-metal aluminides, study in other system[19] showed the orthogonal stress may have considerable effects on the theoretical strength. In the recent study on the hydrostatic tension,[20] the theoretical strength of NiAl was calculated to be 25.6 GPa, significantly lower than 45.4 GPa in uniaxial tension.[6]

B. Implications for experiments

The ideal elastic deformation behaviors, specifically, the failure modes under the ⟨100⟩ uniaxial tension, of the perfect FeAl and NiAl are now discussed. Suppose a perfect crystal is pulled in tension. The crystal may fail by either tension or shear. The failure mode of the material depends on which type of instability is encountered first. It is of interest to distinguish two types of failure modes, i.e., tension and shear, as they give rise to different deformation behaviors. A break in the tensile stability would probably result in cleavage whereas an instability in shear may homogeneously nucleate defects such as dislocations. With the calculated ideal strengths in both uniaxial tension and shear, one can assess the competition between the two modes simply by resolving the ideal tensile strength onto the slip systems and comparing with the ideal shear strengths.

Table II summarizes such comparisons for FeAl and NiAl. In NiAl, the ideal shear strengths on {112}⟨111⟩ easy and {110}⟨111⟩ are well below the relevant resolved shear

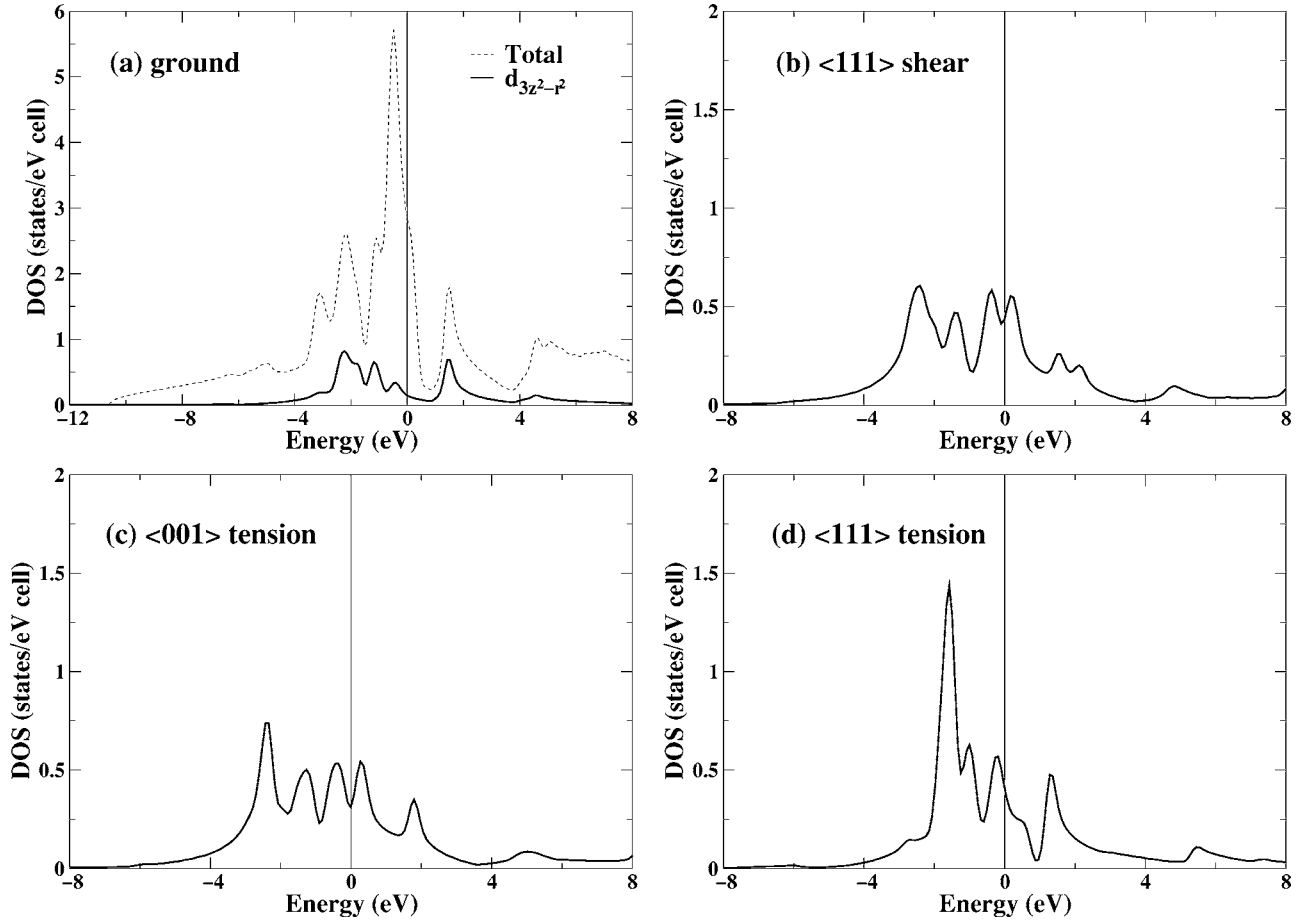

FIG. 4. Calculated projected density of states for the $d_{3z^2-r^2}$ orbitals in FeAl at (a) ground state, and at instabilities for (b) $(1\bar{1}0)[111]$ shear, (c) [001] tension, and (d) [111] tension. A total density of state is also given in (a).

stresses, implying slip may intrude prior to tensile instability even when pulled along ⟨100⟩. In contrast, FeAl is most likely to fail simply in tension due to the opposite relationship between the resolved shear stresses and the theoretical shear strengths. Nevertheless, a certain degree of the ambiguity exists in such a straightforward comparisons, i.e., the resolved shear stresses are not uniaxial and the presence of the orthogonal stress components may affect the maximum strength level. Further, the present model neglects the kinetics of defect mediated slip. However, a strict conclusion regarding the competition between tension and shear can be drawn from the analysis of the internal stability conditions.

TABLE II. Ideal shear strength of NiAl and FeAl for {112}⟨111⟩ and {110}⟨111⟩ shear and the maximum resolved shear stress from ⟨100⟩ tension.

			Resolved shear stress on	
		Ideal strength	{112}⟨111⟩	{110}⟨111⟩
NiAl	⟨100⟩ tension	45.4[a]	21.4	18.5
	{112}⟨111⟩ "easy"	9.3	9.3	
	{110}⟨111⟩	10.3		10.3
FeAl	⟨100⟩ tension	18.6[a]	8.8	7.6
	{112}⟨111⟩ "easy"	13.9	13.9	
	{110}⟨111⟩	15.7		15.7

[a]From Ref. 6.

The elastic instability in FeAl under such examination is clearly seen in Fig. 5(a) at around 14% strain where the eigenvalue that reads $1/2[\lambda_{11}+\lambda_{22}+\lambda_{23}-\sqrt{8\lambda_{12}^2+(\lambda_{22}+\lambda_{23}-\lambda_{11})^2}]$, suddenly falls to zero. It then follows $\lambda_{11}(\lambda_{22}+\lambda_{23})=2\lambda_{12}^2$ at this point. Since the modulus that governs a fully relaxed stretch along this direction is

$$E_{100}=\frac{\lambda_{11}(\lambda_{22}+\lambda_{23})-2\lambda_{12}^2}{\lambda_{22}+\lambda_{23}}.$$

Such instability explicitly corresponds to a failure in tension. In contrast, the same eigenvalue stays positive for NiAl until the corresponding tensile stress-strain curve reaches its maximum. However, at 38% strain [Fig. 5(b)], another eigenvalue $C44$, which has an eigenvector corresponding to shear on ⟨010⟩ direction, vanishes giving rise to a shear instability. It thus follows the same conclusion: a failure in shear instead of tension would take place in "perfect" NiAl under the uniaxial ⟨100⟩ stretch.

Finally, it is interesting to compare the ideal strengths predicted by *ab initio* techniques with experiments. Although making an explicit comparison is usually not feasible due to

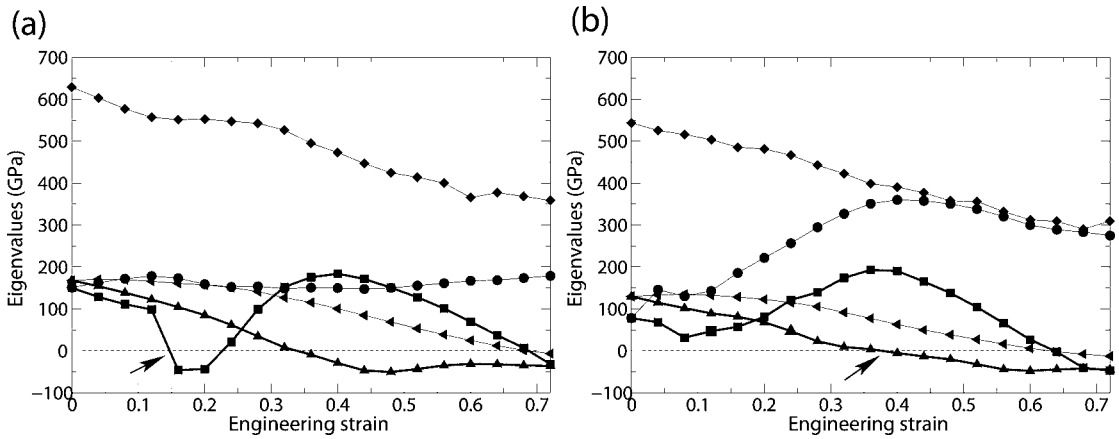

FIG. 5. Eigenvalues of symmetric Wallace tensor as functions of strain for the uniaxial ⟨100⟩ tension in (a) FeAl and (b) NiAl. Six eigenvalues are represented as follows: ∘ for $\lambda_{22}-\lambda_{23}$; □ for $1/2[\lambda_{11}+\lambda_{22}+\lambda_{23}-\sqrt{8\lambda_{12}^2+(\lambda_{22}+\lambda_{23}-\lambda_{11})^2}]$; ◇ for $1/2[\lambda_{11}+\lambda_{22}+\lambda_{23}+\sqrt{8\lambda_{12}^2+(\lambda_{22}+\lambda_{23}-\lambda_{11})^2}]$; △ for λ_{44}; ◁ for λ_{55} (doubly degenerate).

the extreme difficulty in measuring the ideal strength directly, it is of interest to note that experimentally FeAl shows a clear preference for {100} cleavage[1,3] whereas the tensile fracture of ⟨100⟩ single crystal NiAl is associated with {112}⟨111⟩ slip.[21] Both of these observations are in qualitative agreement with predictions based on the ideal strength model. The difference in the cleavage properties of FeAl and NiAl are thus suggested to reflect their intrinsic strength differences. Interestingly, calculations also suggest that FeAl is intrinsically brittle but NiAl is ductile. However, it is found experimentally that both materials are brittle at the room temperature. The source of the discrepancy may reflect the influence from many factors, e.g., the defects, triaxial crack-tip stress state,[19] and kinetic effects on the failure process,[22] that require a more sophisticated model.

IV. CONCLUSIONS

The ideal shear strengths of FeAl and NiAl along ⟨111⟩ direction on {112} and {110} planes are computed and analyzed. Although in NiAl the stress-strain relationship can be understood by the argument based upon the crystal structure transformation, the instabilities in FeAl are actually dictated by filling of the unstable anti-bonding *d* states, that has also been found to account for the intrinsic weakness in ⟨100⟩ tension. The failure modes are examined and differentiated in FeAl and NiAl under the quasi-static ⟨100⟩ uniaxial tension by two methods. Both methods yield the same conclusion that FeAl fails by tension while NiAl fails by shear. The unique electronic instability that appears only in FeAl plays a key role in differentiating the inherent elastic behaviors between the two intermetallics.

ACKNOWLEDGMENTS

This work was supported by the Directorate, Office of Energy Sciences, Office of Basic Energy Sciences, of the Department of Energy under Contract No. DE-AC03-76SF00098 and by National Science Foundation under Grant No. DMR-0304629.

[1] K.-M. Chang, R. Darolia, and H. A. Lipsitt, Acta Metall. Mater. **40**, 2727 (1992).
[2] R. Darolia, K.-M. Chang, and J. E. Hack, Intermetallics **1**, 65 (1993).
[3] M. V. Nathal and C. T. Liu, Intermetallics **3**, 77 (1995).
[4] Peter A. Schultz and James W. Davenport, Scr. Metall. Mater. **27**, 629 (1992).
[5] Peter A. Schultz and James W. Davenport, J. Alloys Compd. **197**, 229 (1993).
[6] Tianshu Li, J. W. Morris, Jr., and D. C. Chrzan, Phys. Rev. B **70**, 054107 (2004).
[7] J. W. Morris, Jr., C. R. Krenn, D. Roundy, and Marvin L. Cohen, in *Phase Transformations and Evolution in Materials* (The Minerals, Metals and Materials Society, Warrendale, PA, 2000), p. 187.
[8] D. Vanderbilt, Phys. Rev. B **41**, R7892 (1990).
[9] G. Kresse and J. Furthmüller, Phys. Rev. B **54**, 11169 (1996).
[10] Hendric J. Monkhorst and James D. Pack, Phys. Rev. B **13**, 5188 (1976).
[11] D. Roundy, C. R. Krenn, Marvin L. Cohen, and J. W. Morris, Jr., Phys. Rev. Lett. **82**, 2713 (1999).
[12] D. Roundy, C. R. Krenn, Marvin L. Cohen, and J. W. Morris, Jr., Philos. Mag. A **81**, 1725 (2001).
[13] Weidong Luo, D. Roundy, Marvin L. Cohen, and J. W. Morris, Jr., Phys. Rev. B **66**, 094110 (2002).
[14] D. B. Miracle, Acta Metall. Mater. **41**, 649 (1993).
[15] J. W. Morris, Jr. and C. R. Krenn, Philos. Mag. A **80**, 2827 (2000).
[16] D. M. Clatterbuck, C. R. Krenn, M. L. Cohen, and J. W. Morris, Jr., Phys. Rev. Lett. **91**, 135501 (2003).

[17] V. Vitek, Philos. Mag. **18**, 154 (1968).
[18] N. I. Medvedeva, O. N. Mryasov, Yu. N. Gornostyrev, D. L. Novikov, and A. J. Freeman, Phys. Rev. B **54**, 13506 (1996).
[19] D. M. Clatterbuck, D. C. Chrzan, and J. W. Morris, Jr., Scr. Mater. **49**, 1007 (2003).
[20] M. Černý, J. Pokluda, and P. Šandera, Mater. Sci. Eng., A **387-389**, 923 (2004).
[21] J. H. Schneibel, R. Darolia, D. F. Lahrman, and S. Schmauder, Metall. Trans. A **24**, 1363 (1993).
[22] Joachim Riedle, Peter Gumbsch, and Hellmut F. Fischmeister, Phys. Rev. Lett. **76**, 3594 (1996).